Article

A scalable and tunable thermoreversible polymer for 3D human pluripotent stem cell biomanufacturing

Thermoreversible Hydrogel Platform

Polymer Synthesis and Material Properties

Liquid — Solid
> LCST
< LCST
25°C — 37°C

- Reproducible
- Fully Defined
- Scalable
- Tunable

Stem Cell Expansion

Self-Renew

hPSCs + Gel

Stem Cell Differentiation

Neurons
Cardiomyocytes
Hepatocytes

Hunter J. Johnson, Saheli Chakraborty, Riya J. Muckom, Nitash P. Balsara, David V. Schaffer

schaffer@berkeley.edu

Highlights
Synthesis of a scalable, tunable, and reproducible thermoreversible hydrogel

Optimization of hydrogel properties including stiffness, LCST, and viscosity

Expansion and pluripotency maintenance of hESCs in the hydrogel platform

Differentiation of neurons, cardiomyocytes, and hepatocytes in the hydrogel platform
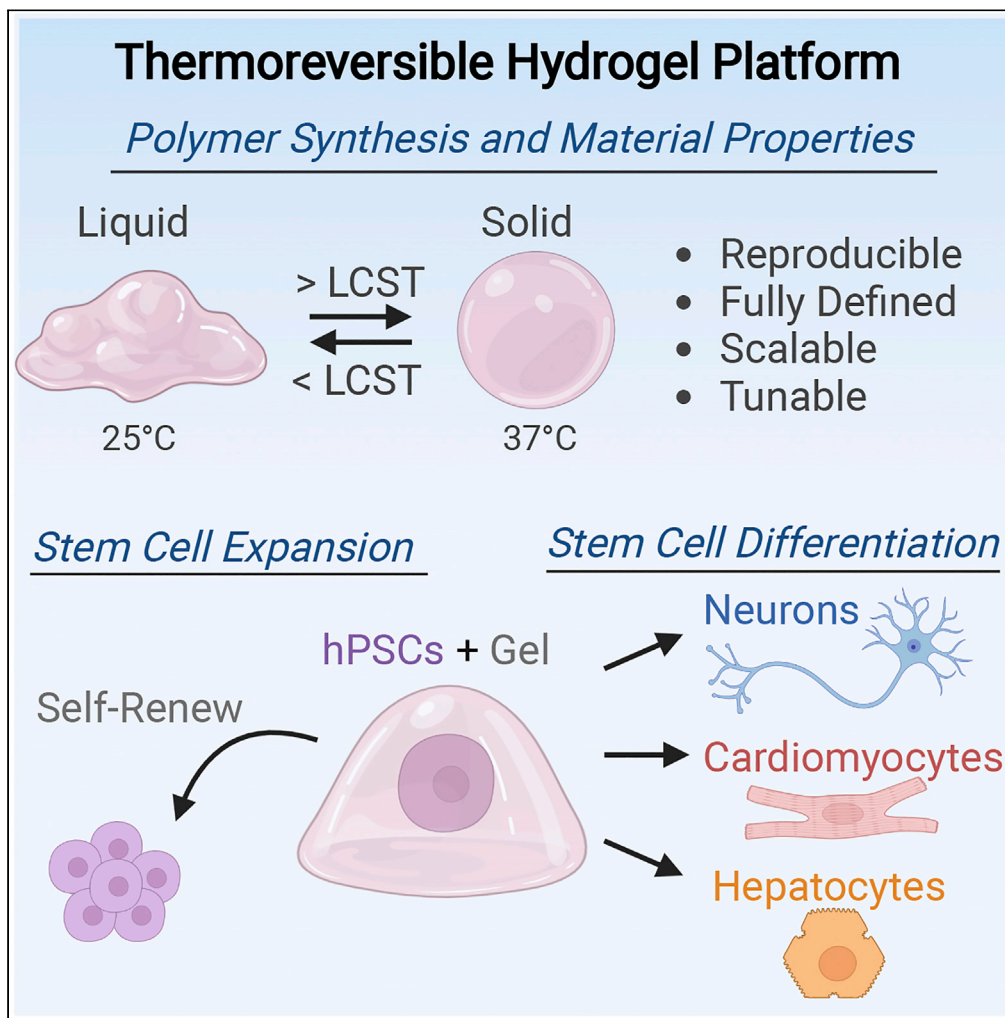
Article

A scalable and tunable thermoreversible polymer for 3D human pluripotent stem cell biomanufacturing

Hunter J. Johnson,[1,2] Saheli Chakraborty,[3] Riya J. Muckom,[4] Nitash P. Balsara,[3,4,5,6] and David V. Schaffer[1,4,7,8,9,*]

SUMMARY

Human pluripotent stem cells (hPSCs) are an exciting and promising source to enable cell replacement therapies for a variety of unmet medical needs. Though hPSCs can be successfully derived into numerous physiologically relevant cell types, effective translation to the clinic is limited by challenges in scalable production of high-quality cells, cellular immaturity following the differentiation process, and the use of animal-derived components in culture. To address these limitations, we have developed a fully defined, reproducible, and tunable thermoreversible polymer for high-quality, scalable 3D cell production. Our reproducible synthesis method enables precise control of gelation temperature (24°C–32°C), hydrogel stiffness (100–4000 Pa), and the prevention of any unintended covalent crosslinking. After material optimization, we demonstrated hPSC expansion, pluripotency maintenance, and differentiation into numerous lineages within the hydrogel. Overall, this 3D thermoreversible hydrogel platform has broad applications in scalable, high-quality cell production to overcome the biomanufacturing burden of stem cell therapy.

INTRODUCTION

Human pluripotent stem cells (hPSCs), including both embryonic (Thomson et al., 1998) and induced (Takahashi et al., 2007), hold immense potential for a variety of biomedical applications, including regenerative medicine, tissue engineering, drug development, toxicity screening, and modeling of human development and disease (Zakrzewski et al., 2019). In particular, given their ability to self-renew indefinitely and derive all cell types of the three germ layers, hPSCs represent an attractive source for cell replacement therapies (CRTs) to treat diseases of degeneration (Bianco and Robey, 2001). Accordingly, there have been numerous reports of defined hPSC differentiation protocols that produce potent and physiologically relevant cell types with supporting preclinical evidence to address unmet medical needs (Keller, 2005; Zakrzewski et al., 2019). However, clinical translation of hPSC-derived cell products will require scalable processes to generate high-quality cells (Alves et al., 2012; Kropp et al., 2017). Degenerative diseases such as myocardial infarction, liver failure, type 1 diabetes, and neurodegenerative disorders can require up to 1×10^9 cells per patient, and considering the patient population and annual incidence may require $>10^{15}$ cells per year for the US alone (Jing et al., 2008). With conventional 2D cell culture, the surface area necessary to produce these cell numbers is prohibitive (Steinbeck and Studer, 2015). Additionally, previous industry-standard 2D culture platforms rely on animal-derived matrix components, such as Matrigel, that introduce hundreds of variable proteins, limit reproducibility, and introduce the safety risks of immunogenic complications in the final cell product (Iaz et al., 2013; Alves et al., 2012). Despite advances for xeno-free and defined 2D hPSC culture methods (Li et al., 2010), there is still a need for scalable methods for hPSC expansion and differentiation, to derive the cell number required for clinical translation.

In contrast to 2D, 3D culture platforms may enable the cellular densities necessary to manufacture hPSCs at scale (Alves et al., 2012). Furthermore, 3D microenvironmental properties including relevant material properties, biochemical cues, and cell-adhesion motifs have also been demonstrated to significantly enhance stem cell expansion, increase differentiation efficiency, and derive more mature and functional cell types compared to 2D culture (Murphy et al., 2014; Lei and Schaffer, 2013). Additionally, several bioreactor compatible 3D culture platforms have been recently developed to address limitations in stem cell biomanufacturing, including microcarrier culture (Badenes et al., 2016), natural and synthetic biomaterial

[1]Department of Bioengineering, University of California, Berkeley, Berkeley, CA 94720, USA

[2]Graduate Program in Bioengineering, University of California, California, San Francisco and University of California, Berkeley, Berkeley, CA 94720, USA

[3]Energy Storage & Distribution Resources Division, Lawrence Berkeley National Laboratory, Berkeley, CA 94720, USA

[4]Department of Chemical and Biomolecular Engineering, University of California, Berkeley, Berkeley, CA 94720, USA

[5]Materials Sciences Division, Lawrence Berkeley National Laboratory, Berkeley, CA 94720, USA

[6]Joint Center for Energy Storage Research, Lawrence Berkeley National Laboratory, Berkeley, CA 94720, USA

[7]Helen Wills Neuroscience Institute, University of California, Berkeley, Berkeley, CA 94720, USA

[8]Department of Molecular and Cell Biology, University of California, Berkeley, Berkeley, CA 94720, USA

[9]Lead contact

*Correspondence: schaffer@berkeley.edu

https://doi.org/10.1016/j.isci. 2022.104971

encapsulation (Xu et al., 2019; Ei et al., 2014), and 3D aggregate suspension (Dahlmann et al., 2013). However, there are limitations with current 3D culture platforms that can limit bioprocessing and feasible scalability of stem cell manufacturing. The use of natural extracellular matrix (ECM) components to coat microcarriers or for biomaterial encapsulation, such as Matrigel, hyaluronic acid, laminin, collagen, and alginate, presents issues with sourcing of human or animal-derived components for scalable manufacturing (Xu et al., 2019). Natural ECM proteins also present lot-to-lot variability (Nicolas et al., 2020). The use of synthetic hydrogels, including PEG-diacrylate and polyacrylamide, may offer a promising approach to 3D cell culture. However, both synthetic and natural ECM-derived hydrogels often rely on covalent crosslinking that can constrain cell expansion and differentiation (Hu et al., 2019). In addition, cellular recover requires harsh enzymatic and mechanical degradation, limiting bioprocessing while also compromising cell health and quality (Xu et al., 2019). Finally, suspension culture of 3D cell aggregates may offer a potential scalable solution to stem cell manufacturing, as there is low cost of goods and high cell yields (Hookway et al., 2016). However, 3D aggregate suspensions require high shear rates in stir-tank reactors to prevent cell agglomeration, affecting cell viability, and differentiation (Rostami et al., 2015).

One material class with significant potential to address the manufacturing needs of hPSC-derived therapies is 3D thermoresponsive hydrogels (Shen et al., 2012; Lei and Schaffer, 2013; McDevitt, 2013). Below their lower critical solution temperature (LCST), thermoreversible polymers are viscous liquids that can be mixed with cells and simply warming the culture vessel above the LCST, to standard cell culture temperatures, induces the formation of physical crosslinks that trigger a sol-gel transition (Xu et al., 2020; Ekerdt et al., 2018). After cells are either expanded or differentiated inside the material, the hydrogel can then be easily liquefied by cooling the culture vessel below the LCST, for collection of the cell product for downstream bioprocessing. Our lab has previously used a commercially available PEG-PNIPAAm block copolymer for hPSC expansion (Lei and Schaffer, 2013) and generation of dopaminergic neurons (Adil et al., 2017), medium spiny neurons (Adil et al., 2018), and oligodendrocyte precursors (Rodrigues et al., 2017) as potential cell therapy candidates for Parkinson disease, Huntington disease, and demyelinating disorders, respectively. This system had the advantage of being synthetic, protecting cells from shear stress, enabling high density cultures, and facilitating easy cellular isolation via temperature cooling for gel liquification. Additionally, both for dopaminergic (Adil et al., 2017) and medium spiny neurons (Adil et al., 2018), the derived cells matured faster and to a greater extent in the 3D hydrogel, in both marker expression and neuronal firing activity. However, standard chemistries to synthesize current PEG-PNIPAAm yield polymers with high batch-to-batch variability, little capacity to tune the cellular microenvironment, and a low LCST, which may complicate downstream bioprocessing. Thus, there is a need for a synthetic and reproducible thermoreversible hydrogel platform with the ability to control temperature and mechanical properties and thereby achieve truly scalable hPSC biomanufacturing.

Here, we describe the development, characterization, and optimization of a fully defined, reproducible, and tunable thermoreversible polymer platform to enable effective hPSC expansion and differentiation at scale. We describe the polymer design and highly reproducible synthesis, demonstrate versatile temperature control of the liquid-solid transition, and explore the mechanical and rheological properties of the material. Furthermore, hPSC viability, expansion, and pluripotency maintenance within the optimized thermoreversible hydrogel are investigated. Finally, we investigated the differentiation potential of hPSCs within the system by deriving potential cell therapy candidates from the three germ layers, namely dopaminergic neurons, cardiomyocytes, and hepatocytes.

RESULTS

Thermoreversible polymer design and synthesis

When conceptualizing the polymer design, we aimed to synthesize a fully defined and synthetic, thermoreversible, random copolymer based on the hydrophilic poly(ethylene glycol) (PEG) and temperature-sensitive poly(N-isopropylacrylamide) (PNIPAAm). Upon heating above the lower critical solution temperature (LCST), the PNIPAAm component becomes increasingly hydrophobic and enables micelle formation, essentially physical "crosslinking" the PEG-PNIPAAm polymer. However, PEG-PNIPAAm alone has a relatively high LCST (33°C) and decreased long-term stability in aqueous solutions at 37°C (Xu et al., 2020). Previous iterations of PEG-PNIPAAm polymers have introduced temperature modulation by introducing methacrylate groups with hydrophobic pendants during polymerization (Yoshioka et al., 1994); however, we found that one-pot polymerization did not yield the desired copolymer, as it had inconsistent methacrylate incorporation as well as the potential for unintended methacrylate crosslinking in storage (data not
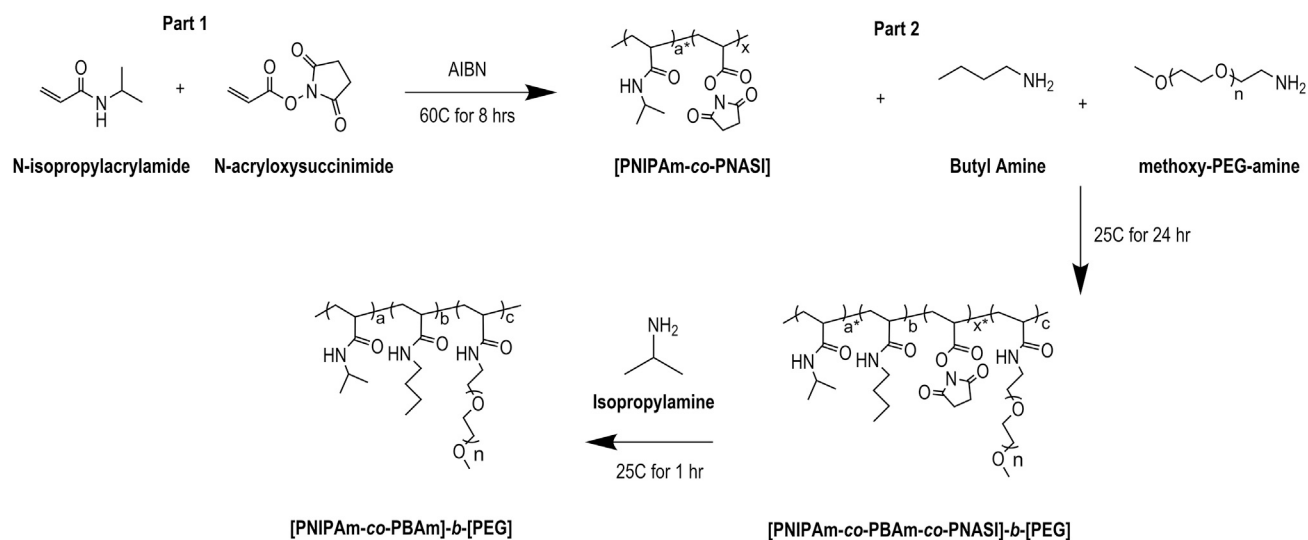
Figure 1. Thermoreversible graft copolymer (GCP) synthesis
Synthesis schematic detaining a two-step reaction to produce the final poly(NIPAAm-co-BAm)-b-PEG graft copolymer. Mole ratios denoted by lowercase between intermediate reactions. AIBN refers to Azobisisobutyronitrile. Butyl amine is depicted, however, other lower alkyl amines can be substituted in the reaction.

shown). Additionally, we aimed to incorporate the PEG block of the copolymer such that there was no possibility for unwanted chemical crosslinking during synthesis, in an effort to improve reproducibility and scalability of synthesis.

A prior PEG-PNIPAAm hydrogel formulation (Yoshioka et al., 1994) has been used in a variety of cell culture applications; however, as with other PEG-PNIPAAm polymers, the product suffers from batch-to-batch variability. In our experience, among a number of independent lots, we have measured substantially different transition temperatures (Figure S1A) and variable final polymer stiffness (Figure S1B). These discrepancies translated to substantial variability in cellular performance and in some cases toxicity (Figure S1C). We attribute this difference, in part, due to a polymer synthesis scheme that is subject to variability in the incorporation of hydrophobic monomers during polymerization and the potential for unintentional chemical crosslinking with diamino-PEG (Yoshioka et al., 1994).

To address these concerns, we developed a two-step synthesis process (Figure 1) to produce a novel thermoreversible graft copolymer, where the PEG represents the hydrophilic block, the PNIPAAm represents the hydrophobic block, and the alkyl pendant group (here described as butyl chains but could encompass any alkyl chain) serves as the temperature shifting moiety. To generate the thermoreversible graft copolymer, a mixture of NIPAAm and N-acryloxysuccinimide (NASI) was first copolymerized via standard radical polymerization. The resulting functionalizable copolymer, after reprecipitation and drying, was then mixed with an amine-terminated alkyl group (here, butylamine) and a monoamine-terminated PEG block. Both amine-terminated groups attached to the PNIPAAm-co-PNASI backbone via the amine and N-hydroxysuccinimide (NHS) amidation reaction. Finally, the remaining NHS groups were converted to NIPAAm via addition of isopropylamine, and the resulting polymer was dried, dialyzed, and lyophilized. H-NMR characterization of the final polymer (Figure S2A) demonstrated the presence of the PNIPAAm, PEG, and butylamine. In addition, GPC characterization (Figure S2B) indicated a polydispersity index (PDI) of 3, with clear lower molecular weight cutoff due to the dialysis. The final thermoreversible graft copolymer was then reconstituted in defined cell culture medium at the desired weight percent for further material characterization and cell culture.

Material properties and optimization of the thermoreversible polymer

After designing the synthetic strategy for the thermoreversible graft copolymer, we investigated key material properties of the hydrogel, as well as optimized material formulations to support hPSC expansion and differentiation.
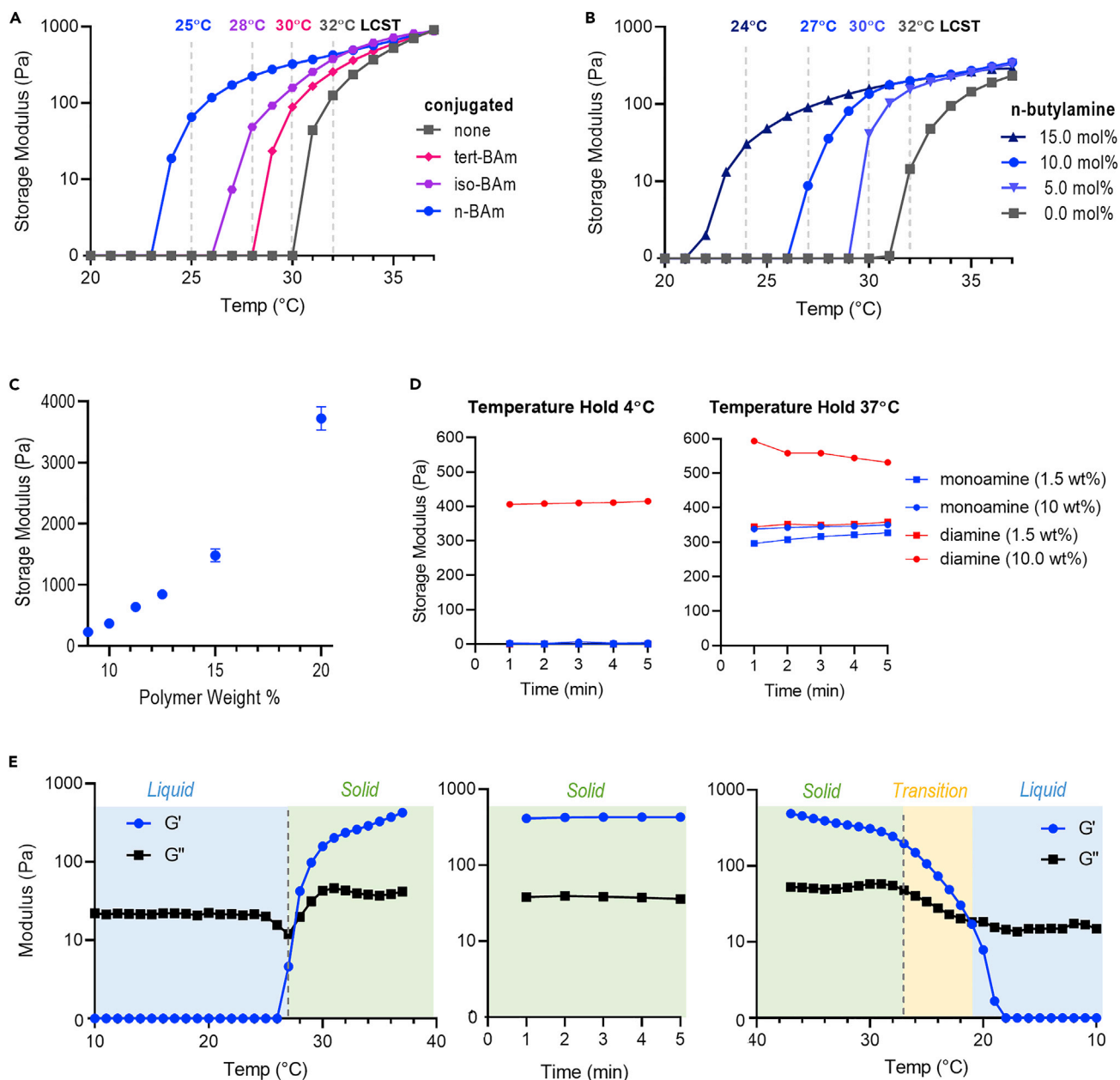
Figure 2. Thermoreversible hydrogel material properties

(A) Rheometry data depicting gelation temperature and hydrogel stiffness with differing structures of added butylamine. The polymers were tested at a constant 12.5 wt % in DMEM/F12, and the butylamine amount was kept constant at a 10 mol % addition.

(B) Rheometry data depicting the shift of gelation temperature and hydrogel stiffness with varying amounts of conjugated n-butylamine. The polymers were tested at a constant 11.0 wt % in DMEM/F12.

(C) Final hydrogel stiffness with varying weight percent (wt %), tested after 5 min of maintenance at 37°C, n = 5, error bars = std. dev.

(D) Final hydrogel stiffness at variable temperatures for mono vs diamino-PEG-conjugated polymers.

(E) Rheometry data depicting temperature ramp up to 37°C, held constant at 37°C, and ramped down to 10°C.

First, we investigated the role of the pendant alkyl group structure on polymer LCST (Figure 2A). Using frequency sweep rheometry, we tracked the temperature transition from liquid (G' = 0), to gelation (G' > G''), to final hydrogel at 37°C (G' ~ 1000 Pa) at various polymer compositions. Maintaining a constant polymer weight percent (wt %) and species mole percent (mol %), we found that the incorporation of an n-butyl acrylamide exerted the greatest effect on LCST, shifting from 32°C with no substitutions to 25°C with

10 mol% n-butylamine. By comparison, iso-butylamine (28°C) and tert-butylamine (30°C) led to intermediate LCSTs. This ordering of LCSTs matches the predicted contributions of these different butyl structures to hydrophobicity. From this initial data, we proceeded with butylamine.

Next, we investigated the effect of the level of n-butylamine incorporation into the thermoreversible graft copolymer by varying the mol % of the compound added during synthesis (Figure 2B). As anticipated, we observed a reduction in the LCST with increasing n-butylamine mol % during synthesis. In particular, scanning from 0–15 mol % n-butylamine enabled a temperature shifting range from 32°C–24°C. When designing the polymer for end application, we selected an LCST slightly above room temperature, 27°C, corresponding to 10 mol % butylamine, as liquid handling of the cell-polymer solution would be ideally performed at this temperature. We then investigated the role of polymer wt % on final gel stiffness and observed a dynamics stiffness range between ∼100 Pa and ∼4000 Pa (Figure 2C), which encompasses stiffnesses we have previously used to culture hPSCs (Adil et al., 2017).

To investigate the effect of using monoamine-PEG compared to the previously reported diamino-PEG during copolymer synthesis, we varied the PEG concentration in the solvent during synthesis and evaluated the resulting polymer stiffness (Figure 2D). When conjugating PEG to the backbone in dilute conditions (1.5 wt % in solvent), the resulting polymers were liquid at 4°C and hydrogels at 37°C, for both mono and diamino-PEG. At higher reaction concentrations (10 wt % in solvent), the mono-PEG material was again a liquid at 4°C and solid at 37°C with the same final stiffness (∼350 Pa). However, we observed apparent, unintended crosslinking when using diamino-PEG at the higher concentrations, where the resulting material exhibited hydrogel stiffness even at 4°C, indicating permanent covalent crosslinking had occurred and hydrogel liquification was inhibited. This is presumably due to the potential of inter- and intrapolymer crosslinking by the addition of a bifunctional PEG. This background crosslinking also translates to an inconsistent hydrogel stiffness among synthesized batches at 37°C, when both physical and chemical crosslinks are present. This unwanted crosslinking is also observable at the conclusion of the polymer synthesis, where the polymer formed a hydrogel within the reaction solvent (Figure S3). Thus, the use of mono-PEG prevents any unwanted covalent crosslinking and enables consistent hydrogel liquification, whereas diamino PEG induces unwanted crosslinking.

After final chemistry optimization, we investigated the thermoreversible properties of the resulting mono-PEG gel formulation, which achieved the desired LCST and reproducible synthesis (Figures 2E, S4A, and S4B). This material is a liquid below the LCST (G′ < G′′), forms a physical hydrogel (G′ > G′′) at the LCST, exhibits a final gel stiffness at 37°C that we have previously found to be supportive of hPSC culture (Lei and Schaffer, 2013), maintains it stiffness at 37°C, and reliquefies upon cooling below the LCST. Finally, the novel synthetic method, with separate addition of butylamine and monoPEG, improves polymer reproducibility as 6 independent synthesis runs resulted in little variation on final polymer LCST (Figure S4A), consistent final hydrogel stiffness (Figure S4B), and high hPSC viability (Figure S4C).

Thermoreversible hydrogel maintains hESC pluripotency

We next investigated the potential of the thermoreversible graft copolymer to support hPSC expansion and pluripotency over time. Following our standard hPSC culture protocol (Figure 3A), we expanded the hPSCs by seeding initial cell clusters of ∼5 cells (Figure S5A) within the liquid-polymer solution, captured the hPSCs within the 3D hydrogel upon warming of the droplets to 37°C, and expanded the hPSCs to 3D aggregates over 4 days of culture in standard pluripotency maintenance medium. We then collected the hPSC aggregates by cooling the culture vessel below the LCST, dissociated the aggregates, and repeated this cycle through 5 passages. The hPSCs exhibited a spherical aggregate morphology by day 4 for all 5 passages (Figure 3B) with a quantifiable aggregate distribution (Figure S5) and maintained a consistent cell expansion rate over the culture period (Figure 3C). Additionally, pluripotency marker expression was maintained over the culture period, as measured by Sox2 and Oct4 positive staining (Figure 3E) within the 3D hPSC aggregates, comparable to standard 2D hPSC culture on Matrigel. Finally, to confirm pluripotency maintenance over the culture period, we submitted a passage 5 sample for the commercial PluriTest (Figure 3D), which resulted in a passing pluripotency score of 27.05 and a novelty score of 1.39 as compared to the internal iPSC positive control and the differentiated negative control. Finally, we compared the cell expansion (Figure S6A), viability (Figure S6B), and pluripotency marker expression for Oct4 (Figure S6C) and Sox2 (Figure S6D) between three different hPSC cell lines over one passage. After one passage, no
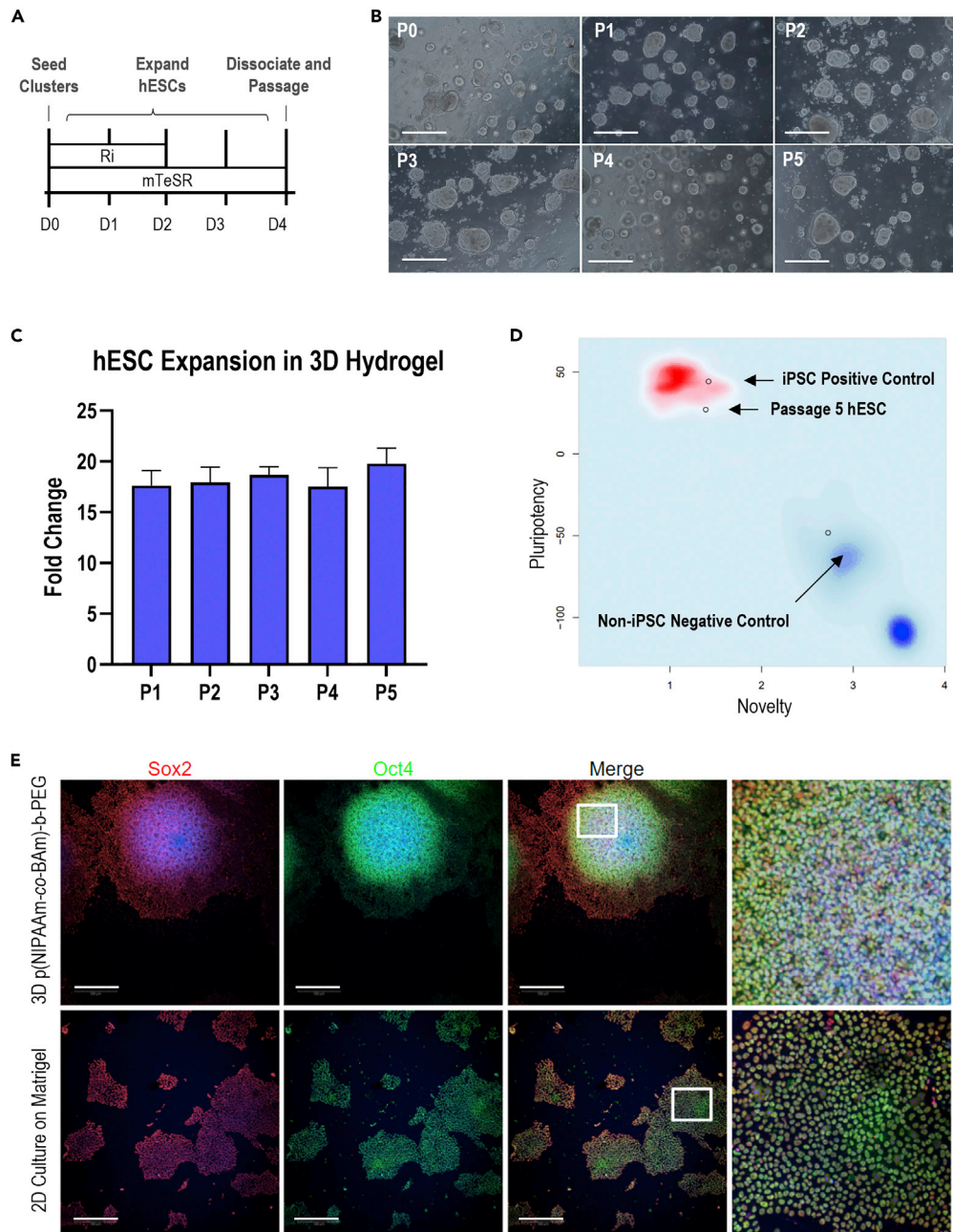
Figure 3. hPSC expansion in the thermoreversible hydrogel

(A) Experiment schematic of hPSC expansion for each passage. Ri = Rock Inhibitor (Y-27632). Further details in STAR Methods.

(B) Representative images of stem cell aggregates within the thermoreversible hydrogel by day 4 of each passage. All scale bars = 100 uM.

(C) hPSC fold change after 4 days of culture in each passage, between seeding count and final cell count. n = 3. Data are represented as mean +/− SD.

(D) PluriTest results of hPSCs maintained in the thermoreversible hydrogel for 5 passages.

(E) Representative images of hPSCs maintained for 5 passages in either the 3D thermoreversible hydrogel or 2D Matrigel. Scale bar = 100 μm. p < 0.05 was considered statistically significant (N.S. p > 0.05, *p < 0.05, **p < 0.01, ***p < 0.001).

statistically significant differences were detected between the three hPSC lines, for expansion, viability, or marker expression, indicating consistent cell performance over multiple lines. Overall, the thermoreversible polymer enables high-quality stem cell expansion and pluripotency maintenance.

Thermoreversible hydrogel supports hESC differentiation

We next investigated the capacity of the material to support the differentiation of hPSCs into potential cell therapy candidates from the three germ layers, namely dopaminergic (mDA) neurons (ectoderm), cardiomyocytes (mesoderm), and hepatocytes (endoderm). First, we directed hPSCs into midbrain dopaminergic neurons within the thermoreversible hydrogel by matching the initial seeding, media components, and timing as our earlier report (Figure 4A; Adil et al., 2017), which had previously adapted this differentiation from 2D (Kriks et al., 2011) to 3D. After 25 days of differentiation, we investigated the presence of mDA markers including FoxA2, tyrosine hydroxylase (TH), and Tuj1 via immunocytochemistry (Figure 4B), where we observed positive marker expression within the 3D aggregates. Flow cytometry analysis showed similar levels of marker expression for 3D defined culture compared to 2D Matrigel, with ∼80% FoxA2 and Tuj1 expression, followed by near 50% TH + expression (Figure 4C). The TH + cells are double-positive for Tuj1+, as indicated by flow cytometry (Figure S7), indicating additional TH- neuronal lineages are present at the end of differentiation. The remaining ∼20% FoxA2-/Tuj1-/TH- population may be neural progenitors or non-neuronal lineage, as reported in other differentiation protocols (Ganat et al., 2012). When comparing the cell production capacity of either culture method (Figure 4D), with matched culture volume, we observe a clear increase in cellular fold change with respect to matched initial seeding conditions between the 2D Matrigel (∼15-fold) and 3D thermoreversible hydrogel culture (∼60-fold). The cellular fold change is defined as the ratio of total differentiated cell number, including marker positive and off target cells, to the initial seeding density at the end of the differentiation protocol.

To investigate mesodermal differentiation potential, we adapted a standard 2D cardiomyocyte differentiation protocol (Lian et al., 2012) to defined 3D differentiation within the thermoreversible hydrogel (Figure 4E). After 15 days, we stained for cardiomyocytes markers cardiac troponin T (cTnT) and α-Actinin (α-Act) (Figure 4F) and observed clear regions of dual marker expression that corresponded to sites of spontaneous contraction within the aggregates (Video S1). We assessed the differentiation efficiency via flow cytometry (Figure 4G), including an additional ventricular marker, myosin light chain-2 (MLC2v), and observed comparable differentiation efficiencies in the 3D thermoreversible polymer as in the standard 2D culture, with both culture methods producing ∼90% cTnt + population. Interestingly, we observed a decrease in the α-Act + population between 2D and 3D, dropping from ∼90% to ∼70%, and an increase in the MLC2v + population between 2D and 3D, rising from ∼45% to 60%. This may represent a switch from atrial to ventricular cardiomyocyte commitment between the two methods. Similarly, we also observed a clear increase in total differentiated cell production between 2D (∼18-fold) to 3D (∼55-fold) by day 15, with matched initial cell seeding numbers (Figure 4H).

Finally, to investigate endodermal differentiation potential, we adapted a standard 2D hepatocyte differentiation protocol (Si-Tayeb et al., 2010) to defined 3D differentiation within the thermoreversible hydrogel system (Figure 4I). After 13 days, we stained for hepatocyte markers alpha fetoprotein (AFP) and hepatocyte nuclear factor alpha (HNF4α) and observed clear nuclear expression for both markers, with a larger proportion of AFP expressing cell types throughout the 3D aggregate. (Figure 4J). Flow cytometry analysis of both hepatocyte markers demonstrated comparable AFP expression values between 2D and 3D culture (∼85%), with a lower HNF4a + percentage in the 3D thermoreversible gel compared to standard 2D Matrigel culture (Figure 4K). The 3D hydrogel approach outperformed 2D (∼10-fold) in total differentiated cell production levels (Figure 4L), with a marked increase cell fold change (∼35-fold) by day 13. Overall, the 3D thermoreversible hydrogel platform successfully supported hPSC differentiation into key clinically relevant cell types of the three germ layers, with comparable differentiation efficiencies to standard 2D culture and robust increase in matched total cell production levels.

DISCUSSION

Human pluripotent stem cells offer immense potential for a variety of biomedical applications, including cell replacement therapy, disease modeling, and tissue engineering. However, there is a need for scalable production of hPSC-derived products. Recent technologies aiming for scalable expansion are limited by animal-derived components, human sourced proteins, design complexity, dimensionality, challenges with cell recovery, low cell expansion, and cost of production. Here, we report the development of a 3D, fully defined, fully synthetic, and tunable thermoreversible hydrogel for the scalable biomanufacturing of hPSCs. Our novel polymer synthesis strategy allows the precise control of gelation temperature (24°C–32°C), stiffness (100–4000 Pa), and reproducible polymer production. Additionally, cell retrieval is simplified to cooling of the thermoreversible gel to release the cultured hPSC-derived product. We have
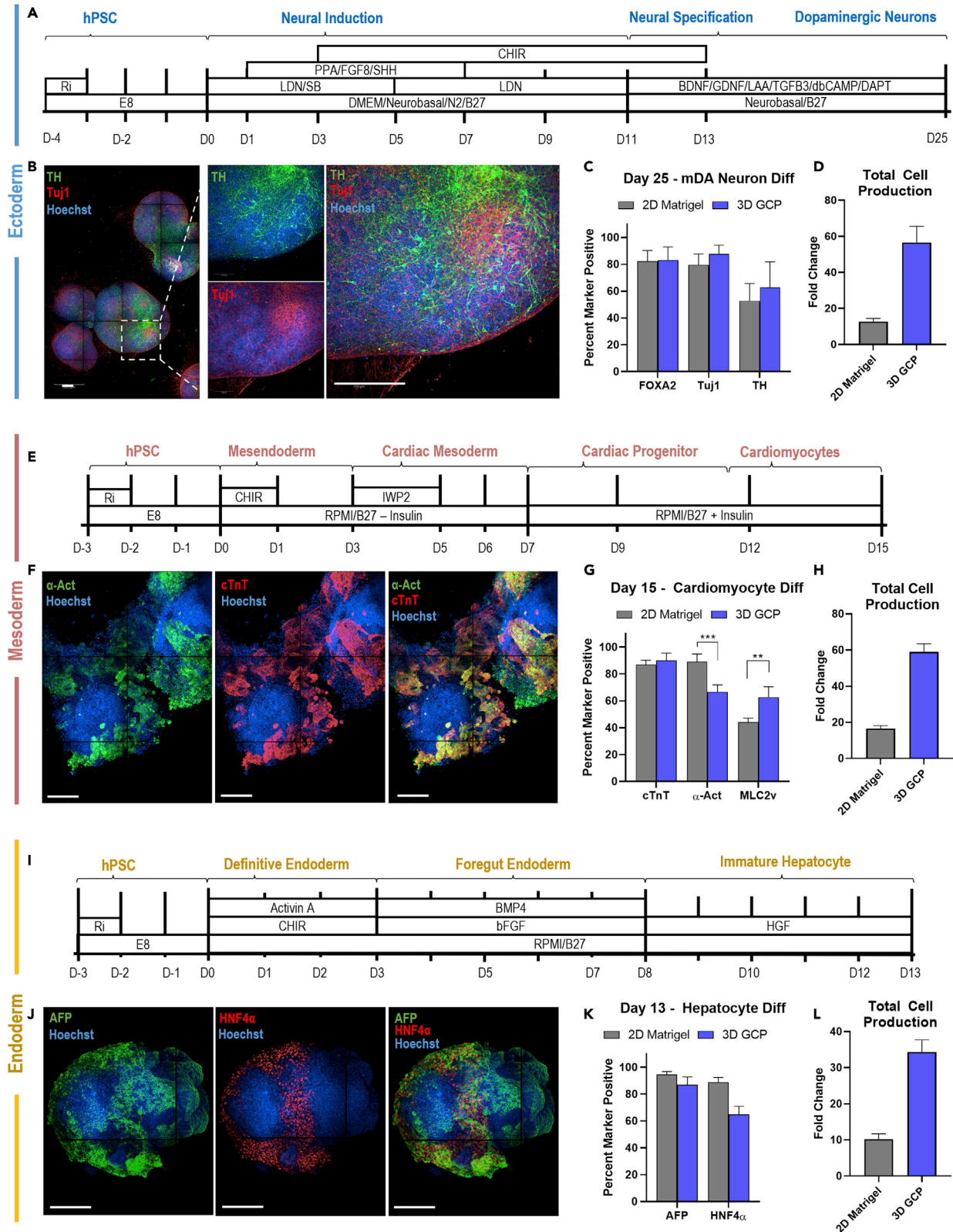
A hPSC — Neural Induction — Neural Specification — Dopaminergic Neurons

Ectoderm / Ectoderm

B TH / Tuj1 / Hoechst

C Day 25 - mDA Neuron Diff

D Total Cell Production

E hPSC — Mesendoderm — Cardiac Mesoderm — Cardiac Progenitor — Cardiomyocytes

Mesoderm

F α-Act / Hoechst; cTnT / Hoechst; α-Act / cTnT / Hoechst

G Day 15 - Cardiomyocyte Diff

H Total Cell Production

I hPSC — Definitive Endoderm — Foregut Endoderm — Immature Hepatocyte

Endoderm

J AFP / Hoechst; HNF4α / Hoechst; AFP / HNF4α / Hoechst

K Day 13 - Hepatocyte Diff

L Total Cell Production

Figure 4. hPSC differentiation in the thermoreversible hydrogel, refered to as 3D graft copolymer (GCP)

(A) Schematic of dopaminergic neuron differentiation, adapted from (Adil et al., 2017).

(B) Representative stained images of day 25 3D aggregates after dopaminergic neuron differentiation.

(C) Flow cytometry analysis of dopaminergic neuron markers at day 25. n = 3.

(D) Total cellular production by day 25 of dopaminergic neuron differentiation. n = 3.

(E) Schematic of cardiomyocyte differentiation, adapted from (Lian et al., 2012).

(F) Representative images of day 15 3D aggregates after cardiomyocyte differentiation.

(G) Flow cytometry analysis of cardiomyocyte markers at day 15. n = 3.

(H) Total cellular production by day 15 of cardiomyocyte differentiation. n = 3.

(I) Schematic of hepatocyte differentiation, adapted from (Si-Tayeb et al., 2010).

(J) Representative images of day 13 3D aggregates after hepatocyte differentiation.

(K) Flow cytometry analysis of hepatocyte markers at day 13. n = 3.

(L) Total cellular production by day 14 of hepatocyte differentiation n = 3.

Data are represented as mean +/− SD. All scale bars = 200 μm. $p < 0.05$ was considered statistically significant (N.S. $p > 0.05$, *$p < 0.05$, **$p < 0.01$, ***$p < 0.001$).

demonstrated strong hPSC viability, expansion, and pluripotency maintenance within the hydrogel, as well as directed differentiation into potential cell therapy candidates from the three germ layers, including dopaminergic neurons (ectoderm), cardiomyocytes (mesoderm), and hepatocytes (endoderm), comparable differentiation efficiency to standard 2D culture methods but substantially improved cell production.

The improved synthetic method and novel polymer structure of the thermoreversible graft copolymer offers key advantages over previous technologies. First, the resulting culture methods are fully defined and do not rely on any animal or human-derived components, enabling cGMP compatibility and regulatory advantages. Secondly, the individual components of this polymer are well characterized and readily available for scale-up synthesis. Third, the addition of the butyl acrylamide after initial polymerization reduced synthesis complexity and allow for more reproducible polymer design and amine incorporation, improving batch-to-batch variability. Fourth, the use of a monoamine-PEG for copolymer grafting prevents any unwanted covalent crosslinking, at any synthesis concentration, improving polymer reproducibly and lowering solvent and vessel volume during polymer scale up.

This reported method relies on standard radical polymerization, and the resulting PDI of the polymer is somewhat broad, at 3, when comparing M_n and M_w, though the resulting hydrogel properties were highly reproducible. Additionally, although the reported polymer was essentially inert to the cells, the free NHS esters after conjugation of the PEG and the butylamine allow for simple functionalization of the polymer with the addition of an amine terminated functional group, such as cysteamine, resulting in a free thiol, or DBCO-amine for copper-free click chemistry. This may be advantageous to provide a bioconjugation site to the thermoreversible polymer for future attachment of growth factors, heparin, peptides, or cell adhesion moieties.

Beyond the proliferation and differentiation studies depicted here, the tunability of the polymer allows for optimizing culture and especially differentiation conditions, by varying stiffness, cellular density, and both timing and composition of media induction to further improve 3D differentiation efficiency. Additionally, there are many other potential cell therapy candidates that may perform well within the material, including pancreatic beta cells for type 1 diabetes, medium spiny neurons for Huntington disease, oligodendrocyte precursors for demyelinating disorders, and many others (Zakrzewski et al., 2019). Finally, this thermoreversible hydrogel system may benefit other scalable cell culture applications in addition to hPSCs, including T cell expansion for oncology, HEK cell expansion for improved production for gene therapies, or even injectable applications (Alexander et al., 2014).

Overall, this novel thermoreversible hydrogel platform is a broadly useful technology for the expansion and differentiation of hPSCs, to enable the clinical translation of hPSC-derived cell therapy candidates.

Limitations of the study

This polymer offers a highly scalable solution to hPSC biomanufacturing, though this study has not yet reported the process development to translate this thermoreversible hydrogel platform to a larger bioreactor system. Additional work involves investigating conditions to dispense the cells and material into the reactor vessel, perfusion of the reactor with the material, whole vessel cooling, and retrieval of the cell product at scale.

Additionally, we only tested one line of hPSCs, the H9 hESC line from WARF, for cellular differentiation, though based on our prior work (Lei and Schaffer, 2013) we anticipate these findings can be extrapolated to other hPSC lines, including iPSCs. We did compare the hPSC expansion capacity within the GCP between two hESC lines and an iPSC line (Figure S6), with comparable cell viability, fold change, and pluripotency marker expression. The result is a broadly useful thermoreversible hydrogel platform.

STAR★METHODS

Detailed methods are provided in the online version of this paper and include the following:

- KEY RESOURCES TABLE
- RESOURCE AVAILABILITY
  - Lead contact
  - Materials availability
  - Data and code availability
- EXPERIMENTAL MODEL AND SUBJECT DETAILS
  - hPSC culture in 2D
  - hPSC expansion in 3D
  - hESC differentiation
- METHOD DETAILS
  - Thermoreversible polymer synthesis
  - GPC and ^{1}H-NMR
  - Rheometry analysis
  - Immunostaining and imaging
  - Flow cytometry and analysis
- QUANTIFICATION AND STATISTICAL ANALYSIS

SUPPLEMENTAL INFORMATION

Supplemental information can be found online at https://doi.org/10.1016/j.isci.2022.104971.

AUTHOR CONTRIBUTIONS

H.J.J. conceived the study, designed and performed the experiments, performed the analysis, visualized and managed the data, and wrote the manuscript. S.C. conceived the study, designed and performed experiments, performed the analysis, and help edit the manuscript. R.J.M. designed and performed the experiments and helped edit the manuscript. D.V.S. conceived the study, designed the experiments, visualized the data, and wrote the manuscript.

DECLARATION OF INTERESTS

H.J.J., S.C., and D.V.S. are co-inventors on related intellectual property. H.J.J., R.J.M., and D.V.S. are co-founders of a stem cell therapy company.

REFERENCES

Adil, M.M., Rodrigues, G.M.C., Kulkarni, R.U., Rao, A.T., Chernavsky, N.E., Miller, E.W., and Schaffer, D.V. (2017). Efficient generation of hPSC-derived midbrain dopaminergic neurons in a fully defined, scalable, 3D biomaterial platform. Sci. Rep. 7, 40573. https://doi.org/10.1038/srep40573.

Adil, M.M., Gaj, T., Rao, A.T., Kulkarni, R.U., Fuentes, C.M., Ramadoss, G.N., Ekman, F.K., Miller, E.W., and Schaffer, D.V. (2018). hPSC-derived striatal cells generated using a scalable 3D hydrogel promote recovery in a Huntington disease mouse model. Stem Cell Rep. 10, 1481–1491. https://doi.org/10.1016/j.stemcr.2018.03.007.

Alexander, A., et al. (2014). Polyethylene glycol (PEG)-Poly(N-isopropylacrylamide) (PNIPAAm) based thermosensitive injectable hydrogels for biomedical applications. Eur. J. Pharm. Biopharm. 88, 575–585. https://doi.org/10.1016/j.ejpb.2014.07.005.

Serra, M., Brito, C., Correia, C., and Alves, P.M. (2012). Process engineering of human pluripotent stem cells for clinical application. Trends Biotechnol. 30, 350–359. https://doi.org/10.1016/j.tibtech.2012.03.003.

Badenes, S.M., et al. (2016). Microcarrier-based platforms for in vitro expansion and differentiation of human pluripotent stem cells in bioreactor culture systems. J. Biotechnol. 234, 71–82. https://doi.org/10.1016/j.jbiotec.2016.07.023.

Bianco, P., and Robey, P.G. (2001). Stem cells in tissue engineering. Nature 414, 118–121.

Dahlmann, J., Kensah, G., Kempf, H., Skvorc, D., Gawol, A., Elliott, D.A., Dräger, G., Zweigerdt, R., Martin, U., and Gruh, I. (2013). The use of agarose microwells for scalable embryoid body formation and cardiac differentiation of human and murine pluripotent stem cells. Biomaterials 34, 2463–2471. https://doi.org/10.1016/j.biomaterials.2012.12.024.

Lei, Y., Jeong, D., Xiao, J., and Schaffer, D.V. (2014). Developing defined and scalable 3D culture systems for culturing human pluripotent stem cells at high densities. Cell. Mol. Bioeng. 7, 172–183. https://doi.org/10.1007/s12195-014-0333-z.

Ekerdt, B.L., Fuentes, C.M., Lei, Y., Adil, M.M., Ramasubramanian, A., Segalman, R.A., and Schaffer, D.V. (2018). Thermoreversible hyaluronic acid-PNIPAAm hydrogel systems for 3D stem cell culture. Adv. Healthc. Mater. 7. e1800225–12. https://doi.org/10.1002/adhm.201800225.

Ganat, Y.M., Calder, E.L., Kriks, S., Nelander, J., Tu, E.Y., Jia, F., Battista, D., Harrison, N., Parmar, M., Tomishima, M.J., et al. (2012). Identification of embryonic stem cell-derived midbrain dopaminergic neurons for engraftment. J. Clin. Invest. 122, 2928–2939. https://doi.org/10.1172/JCI58767.

Hookway, T.A., et al. (2016). Aggregate formation and suspension culture of human pluripotent stem cells and differentiated progeny. Methods 101, 11–20. https://doi.org/10.1016/j.ymeth.2015.11.027.

Hu, W., Wang, Z., Xiao, Y., Zhang, S., and Wang, J. (2019). Advances in crosslinking strategies of biomedical hydrogels. Biomater. Sci. 7, 843–855. https://doi.org/10.1039/c8bm01246f.

Villa-Diaz, L.G., Ross, A.M., Lahann, J., and Krebsbach, P.H. (2013). Concise review : the evolution of human pluripotent stem cell culture : from feeder cells to synthetic coatings. Stem Cells 31, 1–7. https://doi.org/10.1002/stem.1260.

Jing, D., et al. (2008). Stem cells for heart cell therapies. Tissue Eng. B 14, 393–406.

Keller, G. (2005). Embryonic stem cell differentiation: emergence of a new era in biology and medicine. Genes Dev. 19, 1129–1155. https://doi.org/10.1101/gad.1303605.

Kriks, S., Shim, J.W., Piao, J., Ganat, Y.M., Wakeman, D.R., Xie, Z., Carrillo-Reid, L., Auyeung, G., Antonacci, C., Buch, A., et al. (2011). Dopamine neurons derived from human ES cells efficiently engraft in animal models of Parkinson's disease. Nature 480, 547–551. https://doi.org/10.1038/nature10648.

Kropp, C., Massai, D., and Zweigerdt, R. (2017). Progress and challenges in large-scale expansion of human pluripotent stem cells. Pro. Biochem. 244–254. https://doi.org/10.1016/j.procbio.2016.09.032.

Lei, Y., and Schaffer, D.V. (2013). A fully defined and scalable 3D culture system for human pluripotent stem cell expansion and differentiation. Proc. Natl. Acad. Sci. USA 110, E5039–E5048. https://doi.org/10.1073/pnas.1309408110.

Li, J., Bardy, J., Yap, L.Y.W., Chen, A., Nurcombe, V., Cool, S.M., Oh, S.K.W., and Birch, W.R. (2010). Impact of vitronectin concentration and surface properties on the stable propagation of human embryonic stem cells. Biointerphases 5, FA132–FA142. https://doi.org/10.1116/1.3525804.

Lian, X., Hsiao, C., Wilson, G., Zhu, K., Hazeltine, L.B., Azarin, S.M., Raval, K.K., Zhang, J., Kamp, T.J., and Palecek, S.P. (2012). Robust cardiomyocyte differentiation from human pluripotent stem cells via temporal modulation of canonical Wnt signaling. Proc. Natl. Acad. Sci. USA 109, E1848–E1857. https://doi.org/10.1073/pnas.1200250109.

McDevitt, T.C. (2013). Scalable culture of human pluripotent stem cells in 3D. Proc. Natl. Acad. Sci. USA 110, 20852–20853. https://doi.org/10.1073/pnas.1320575111.

Murphy, W.L., Mcdevitt, T.C., and Engler, A.J. (2014). Materials as stem cell regulators. Nat. Mater. 13, 547–557. https://doi.org/10.1038/NMAT3937.

Nicolas, J., Magli, S., Rabbachin, L., Sampaolesi, S., Nicotra, F., and Russo, L. (2020). 3D extracellular matrix mimics: fundamental concepts and role of materials chemistry to influence stem cell fate. Biomacromolecules 21, 1968–1994. https://doi.org/10.1021/acs.biomac.0c00045.

Rodrigues, G.M.C., Gaj, T., Adil, M.M., Wahba, J., Rao, A.T., Lorbeer, F.K., Kulkarni, R.U., Diogo, M.M., Cabral, J.M.S., Miller, E.W., et al. (2017). Defined and scalable differentiation of human oligodendrocyte precursors from pluripotent stem cells in a 3D culture system. Stem Cell Rep. 8, 1770–1783. https://doi.org/10.1016/j.stemcr.2017.04.027.

Rostami, M.R., Wu, J., and Tzanakakis, E.S. (2015). Inverse problem analysis of pluripotent stem cell aggregation dynamics in stirred-suspension cultures. J. Biotechnol. 208, 70–79. https://doi.org/10.1016/j.jbiotec.2015.05.018.

Shen, Z., Bi, J., Shi, B., Nguyen, D., Xian, C.J., Zhang, H., and Dai, S. (2012). Exploring thermal reversible hydrogels for stem cell expansion in three-dimensions. Soft Matter 8, 7250–7257. https://doi.org/10.1039/c2sm25407g.

Si-Tayeb, K., Noto, F.K., Nagaoka, M., Li, J., Battle, M.A., Duris, C., North, P.E., Dalton, S., and Duncan, S.A. (2010). Highly efficient generation of human hepatocyte-like cells from induced pluripotent stem cells. Hepatology 51, 297–305. https://doi.org/10.1002/hep.23354.

Steinbeck, J.A., and Studer, L. (2015). Moving stem cells to the clinic : potential and limitations for brain repair. Neuron 86, 187–206. https://doi.org/10.1016/j.neuron.2015.03.002.

Takahashi, K., Tanabe, K., Ohnuki, M., Narita, M., Ichisaka, T., Tomoda, K., and Yamanaka, S. (2007). Induction of pluripotent stem cells from adult human fibroblasts by defined factors. Cell 131, 861–872. https://doi.org/10.1016/j.cell.2007.11.019.

Thomson, J.A., Itskovitz-Eldor, J., Shapiro, S.S., Waknitz, M.A., Swiergiel, J.J., Marshall, V.S., and Jones, J.M. (1998). Embryonic stem cell lines derived from human blastocysts. Science 282, 1145–1147.

Xu, X., Liu, Y., Fu, W., Yao, M., Ding, Z., Xuan, J., Li, D., Wang, S., Xia, Y., and Cao, M. (2020). Poly(N-isopropylacrylamide)-Based thermoresponsive composite hydrogels for biomedical applications. Polymers 12, 580–622.

Xu, Y., Chen, C., Hellwarth, P.B., and Bao, X. (2019). Biomaterials for stem cell engineering and biomanufacturing. Bioact. Mater. 366–379. https://doi.org/10.1016/j.bioactmat.2019.11.002.

Yoshioka, H., Mikami, M., Mori, Y., and Tsuchida, E. (1994). A synthetic hydrogel with thermoreversible gelation. I. Preparation and rheological properties. J. Macromol. Sci. Part A 31, 113–120. https://doi.org/10.1080/10601329409349722.

Zakrzewski, W., Dobrzyński, M., Szymonowicz, M., and Rybak, Z. (2019). Stem cells: past, present, and future. Stem Cell Res. Ther. 10, 68. https://doi.org/10.1186/s13287-019-1165-5.

STAR★METHODS

KEY RESOURCES TABLE

REAGENT or RESOURCE	SOURCE	IDENTIFIER
Antibodies		
Goat polyclonal ant-FoxA2 (FC: 1:100)	R&D Systems	Cat#AF2400; RRID:AB_2294104
Rabbit polyclonal ant-Tuj1 (ICC 1:1000, FC: 1:500)	Abcam	Cat#ab18207; RRID:AB_444319
Mouse monoclonal ant-Tyrosine Hydroxylase (TH) (ICC 1:200, FC 1:100)	Millipore Sigma	Cat#MAB318; RRID:AB_2201528
Mouse monoclonal ant-Cardiac Troponin T (cTnt) (ICC 1:1000, FC 1:500)	Abcam	Cat#ab8295; RRID:AB_306445
Mouse monoclonal ant-α-Actinin (α-Actinin) (ICC 1:200, FC 1:100)	Invitrogen	Cat# MA5-36095; RRID:AB_2890273
Rabbit monoclonal anti-Myosin Light Chain 2v (MLC2v) (FC 1:500)	Abcam	Cat#ab79935; RRID:AB_1952220
Mouse monoclonal ant-Alpha fetoprotein (AFP) (ICC 1:200, FC 1:100)	R&D Systems	Cat#MAB1368; RRID:AB_357658
Rabbit monoclonal ant-Hepatocyte Nuclear Factor 4α (HNF4α) (ICC 1:1000, FC: 1:500)	Cell Signaling Technologies	Cat#3113S; RRID:AB_2295208
Experimental models: Cell lines		
Human: Passage 50 H9 ES cells	WiCell	n/a
Human: Passage 55 H1 ES cells	WiCell	n/a
Human: Passage 10 TMOi001-A iPS cells	Gibco	n/a

RESOURCE AVAILABILITY

Lead contact

Further information and requests for resources and reagents should be directed to and will be fulfilled by the lead contact, David V. Schaffer (schaffer@berkeley.edu).

Materials availability

This study did not generate new unique reagents.

Data and code availability

- All data reported in this paper will be shared by the lead contact upon request.

- This paper does not report original code.

- Any additional information required to reanalyze the data reported in this paper is available from the lead contact upon request.

EXPERIMENTAL MODEL AND SUBJECT DETAILS

hPSC culture in 2D

For routine culture and maintenance, hESC lines (H9 and H1, WiCell) and iPSC lines (TMOi001-A, ThermoFisher) were grown on Matrigel (Corning, lot #1313001) coated plates in mTeSR1 medium (STEMCELL Technologies) and 1% penicillin/streptomycin (Life Technologies) at 37°C and 5% CO_2 with daily media changes. For single-cell seeded maintenance or experiments, cells were singularized with Accutase (STEMCELL Technologies) at 37°C for 4 min and seeded onto Matrigel-coated plates in media containing 10 μM ROCK inhibitor Y-27632 (Selleckchem). 6-well plates were utilized for hPSC maintenance while hPSC differentiations were performed on 24-well plates for the 2D conditions. Cells were seeded at a density of 15k cell/cm^2 for maintenance or 35k cells/cm^2 for differentiations (see hPSC differentiation in 2D). For cluster seeded maintenance or experiments, hESCs were collected with Versene (ThermoFisher)

at 37°C for 4 min and were dissociated with a P1000 wide bore pipette (ThermoFisher). Maintenance passages ranged from 1:10-1:12 (~15k cells/cm^2). Cell counts were determined by further trituration and counting on a hemocytometer.

hPSC expansion in 3D

For hPSC expansion within the thermoreversible hydrogel, hESC lines (H9 and H1, WiCell) and iPSC line (TMOi001-A, ThermoFisher) were collected as clusters from standard 2D maintenance (see hESC expansion in 2D) after Versene treatment with a wide-bore pipette. Cell counts were determined by further trituration and counting on a hemocytometer. Clusters were seeded within the liquid state of the hydrogel (on ice) at 1 × 10^6 cells/mL. The working polymer concentration ranged from 10-12.5 wt %, reconstituted in DMEM/F12 (ThermoFisher). Cell and gel suspensions were mixed and seeded as 50 μL droplets in 24WPs and incubated at 37C for 10 min to shift to the gel state. Warmed mTeSR-1 (STEMCELL Technologies) containing 10 μM ROCK inhibitor Y-27632 (Selleckchem) was added to the hydrogels, and the media was changed daily according to the expansion timeline (Figure 3A). To collect and passage the cells, aggregates were dissociated using warmed Accutase for 4 min at 37°C and mechanical dissociation via gentle mixing with a P1000 and P200 pipette. Fold change was determined by diving the final cell number achieved after 4-day of growth by the initial cell seeding number (50k cells). Cells were counted on a hemocytometer and reseeded as 50 uL droplets in 24 well-plates at 1 × 10^6 cells/mL to restart the passage protocol.

hESC differentiation

hESCs were differentiated into cell therapy candidates from the three germ layers, dopaminergic neurons (Adil et al., 2017), cardiomyocytes (Lian et al., 2012), and hepatocytes (Si-Tayeb et al., 2010), following previously published protocols, timing, and factor concentrations (Figures 4A, 4E, and 4I). hESCs were seeded as single cells (35k cells/cm^2) in a 24 well plate for 2D, or single cells in the thermoreversible polymer (50k cells/50 uL gel) in 24 well plate for 3D. The protocol media and timing were held constant between both formats.

For mDA neuron differentiations, the basal medium, timing, and factor additions are described in Figure 4A. Basal media included E8 Essential Medium, DMEM/F12 Basal Medium, Neurobasal Medium, with N2-Supplement 100X or B-27 50X Supplement (all from Thermo Fisher). Differentiation factors and concentrations included LDN-193189 (LDN, 100 nM), SB-431542 (SB, 10 μM), Purmorphamine (PPA, 2 μM), CHIR-99021 (CHIR, 3 μM), dibutyrylcAMP (dbCAMP, 0.5 mM), DAPT (10 μM), (all from Selleckchem), FGF8 (100 ng/mL), BDNF (20 ng/mL), GDNF (20 ng/mL), TGFβ3 (1 ng/mL) (all from Peprotech), and L-Ascorbic Acid (LAA, 0.2 mM, Sigma).

For cardiomyocyte differentiations, the basal medium, timing, and factor additions are described in Figure 4E. Basal media included Essential 8 and RPMI 1640 Medium with B-27 50X Supplement or B-27 50X Supplement Minus Insulin (all from Thermo Fisher). Differentiation factors and concentrations included CHIR-99021 (10 μM) and IWP2 (5 mM) (both from Sellekchem).

For hepatocyte differentiations, the basal medium, timing, and factor additions are described in Figure 4I. Basal media included Essential 8 and RPMI 1640 Medium, with B-27 50X Supplement (all from Thermo Fisher). Differentiation factors and concentrations included CHIR-99021 (3 μM, Sellekchem), Activin A (100 ng/mL), FGF2 (5 ng/mL), BMP4 (20 ng/mL), and HGF (20 ng/mL) (all from Peprotech).

After differentiation, the resulting cell product, in 2D or 3D, were fixed for immunocytochemistry or collected and singularized in Accutase at 37C for 15 min, followed by mechanical disruption with a P1000 pipette, and fixed for flow cytometry. Cell fold change was determined by diving the resulting cell number after differentiation by the seeding cell density, as determined by hemocytometer.

METHOD DETAILS

Thermoreversible polymer synthesis

To synthesize the intermediate copolymer, N-isopropylacrylamide (Sigma) and N-acryloxysuccinimide (Sigma) were dissolved and polymerized via standard radical polymerization with Azobisisobutyronitrile (Sigma) for 8 h at 60°C. The resulting activated copolymer was reprecipitated in anhydrous diethyl ether

(Sigma) and dried overnight. Typical reaction 1 efficiencies >80% yield. Next, the activated copolymer was dissolved with methoxy-PEG-amine (Sigma) and various lower alkyl amines (Sigma) (see Figure 2) and reacted for 24 h at room temperature. Finally, a saturating amount of isopropylamine (Sigma) was added to convert any remaining N-hydroxysuccinimide sites to pNIPAAm The resulting thermoreversible polymer was concentrated, isolated, and dried overnight. Typical reaction 2 efficiencies >90% yield. The polymer product was purified using dialysis, diluted to 2 wt % for sterile filtration (0.22 µm filter), and water was removed via lyophilization. The final polymer structure and material properties were determined via ^{1}H-NMR, GPC, and Rheometry.

GPC and ^{1}H-NMR

The molecular weight of the polymer was determined by gel permeation chromatography (GPC) using an Agilent 1260 Infinity Series instrument, fitted with Waters Styragel HR 3 and HR 4 columns. N-Methyl-2 pyrrolidone (NMP) containing 0.05 M LiBr was used as the mobile phase, and the experiment was conducted at 70°C. The molecular weight was calibrated using PEO standards (Fluka). ^{1}H-NMR was used to analyze the polymer structure, in deuterated chloroform.

Rheometry analysis

Thermoreversible hydrogels were reconstituted after lyophilization between 5 and 20 wt % in DMEM/F12 media (Thermo Fisher) overnight at 4°C, resulting in a viscous liquid. An Anton-Paar MCR 301 rheometer with an 8mm parallel plate was used to assess material properties of the hydrogel. Frequency sweeps and temperature sweeps between 4 and 37°C, with a stepwise increase at 1 °C/min, were utilized to assess thermoreversiblilty and LCST of the polymer. Temperature holds at 4 and 37°C were utilized to assess final polymer stiffness, held for 5 min.

Immunostaining and imaging

For 2D cell cultures, cells were fixed with 4% paraformaldehyde (Thermo Fisher) in PBS for 15 min at room temperature and subsequently washed three times with PBS, followed by blocking and permeabilization with 5% normal donkey serum (Sigma-Aldrich) and 0.3% Triton X-100 (Fisher Scientific) in PBS (PBS-DT) for 1 h. Cells were incubated with primary antibodies (key resources table) at 4°C overnight, then washed three times with PBS, and incubated with fluorescently conjugated secondary antibodies (Thermo Fisher) at 1:250 dilution for 1 h at room temperature. Both primary and secondary antibodies were diluted in PBS. Cells were washed with PBS and stained with 0.1 µg mL $^{-1}$ DAPI nuclear stain (Thermo Fisher) prior to imaging.

For 3D cell cultures in the thermoreversible hydrogel, cell aggregates were collected by removing the culture medium, adding cold PBS, and incubating on ice for 10 min. The hydrogels liquefied, releasing the cell aggregates, which were then collected using a P1000 wide bore pipette and washed with PBS. The 3D aggregates were then fixed in 4% paraformaldehyde (Thermo Fisher) in PBS for 20 min at room temperature and washed three times with PBS. For staining.

Confocal imaging was performed on a Perkin Elmer Opera Phenix system (QB3 High-Throughput Screening Facility). Brightfield and widefield fluorescence imaging was performed on a Zeiss AxioObserver epi-fluorescent microscope and a Molecular Devices Image Xpress Micro imaging system (CIRM/QB3 Shared Stem Cell Facility).

Flow cytometry and analysis

For hESC cultures, single cells were isolated from 2D or 3D with Accutase 37°C for 5 min. For terminally differentiated cell types, single cells were isolated from 2D or 3D with Accutase at 37°C for 10 min followed by 5 min 0.05% Trypsin-EDTA (Thermo Fisher) and washed with culture medium. Single cell suspensions were centrifuged, fixed in 4% paraformaldehyde (Thermo Fisher) in PBS for 15 min at room temperature, and stored in ice-cold 95% methanol (Sigma) in deionized water. For flow analysis, cells were washed three times with PBS, and incubated with primary antibodies (key resources table) at room temp for 1 h in Flow Buffer (0.5% BSA +0.3% Triton X-100 in PBS), then washed three times with PBS, and incubated with fluorescently conjugated secondary antibodies (Thermo Fisher) in Flow Buffer at 1:250 dilution for 30 min at room temperature. Cells were then washed three times with PBS and transferred to flow tubes. Flow analysis and was performed on a Thermo Fisher Attune (CIRM/QB3 Shared Stem Cell Facility). Data analysis was

performed with FlowJo 10 software. Stained hESCs negative controls and isotype controls were included for gating.

QUANTIFICATION AND STATISTICAL ANALYSIS

Data are represented as mean ± 1 SD (SD) unless otherwise specified. Statistical significance was determined by Student's t test (two-tail) between two groups, and three or more groups were analyzed by one-way ANOVA followed by Tukey test for multiple comparisons. $p < 0.05$ was considered statistically significant (NS $p > 0.05$, *$p < 0.05$, **$p < 0.01$, ***$p < 0.001$). Statistical analysis and data plotting was performed in GraphPad Prism.